


Protein arginine methyltransferase 6 enhances immune checkpoint blockade efficacy via the STING pathway in MMR-proficient colorectal cancer

Jinlin Duan,^{1,2} Tao Chen,³ Qiwei Li,³ Yu Zhang,^{4,5} Ting Lu,⁵ Junyan Xue,⁵ Yang Sun,⁵ Ling Gao,¹ Yonglong Zhang ^{6,7}

To cite: Duan J, Chen T, Li Q, *et al.* Protein arginine methyltransferase 6 enhances immune checkpoint blockade efficacy via the STING pathway in MMR-proficient colorectal cancer. *Journal for ImmunoTherapy of Cancer* 2025;**13**:e010639. doi:10.1136/jitc-2024-010639

► Additional supplemental material is published online only. To view, please visit the journal online (<https://doi.org/10.1136/jitc-2024-010639>).

JD, TC and QL contributed equally.

Accepted 26 February 2025



© Author(s) (or their employer(s)) 2025. Re-use permitted under CC BY-NC. No commercial re-use. See rights and permissions. Published by BMJ Group.

For numbered affiliations see end of article.

Correspondence to

Professor Yonglong Zhang;
yonglongzhang@sibcb.ac.cn

Dr Yang Sun;
yangsun0927@163.com

Ling Gao;
gaoling02@suda.edu.cn

ABSTRACT

Background The emergence of immunotherapy has revolutionized the paradigm of cancer treatment with immune checkpoint blockades (ICB) in solid cancers, including colorectal cancer (CRC). However, only a small subset of CRC patients harboring deficient mismatch repair (dMMR) or microsatellite instability-high (MSI-H) benefits from ICB therapy. A very limited response to ICB therapy has been achieved in MMR-proficient CRC, representing a significant challenge limiting the clinical application of immunotherapy. MMR is the critical DNA repair pathway that maintains genomic integrity by correcting DNA mismatches, which is mediated by the MutSα or MutSβ complex consisting of MSH2 with MSH6 and MSH3, respectively. Given that MMR status directs effective immune response, we sought to determine whether targeting MMR capacity boosts ICB efficacy.

Methods Azoxymethane/dextran sodium sulfate (AOM/DSS)-induced CRC and xenograft model were used to evaluate the function of PRMT6 and response to PRMT6 inhibitor EPZ020411 and combination therapy of PD1 and EPZ020411. Biochemical assays were performed to elucidate the underlying mechanism of PRMT6-mediated MSH2 methylation and immune evasion.

Results We have identified PRMT6 as a crucial regulator of MMR capacity via MSH2 dimethylation at R171 and R219. Such a modification abrogates its MMR capacity and prevents the recruitment of MSH3 and MSH6. PRMT6 loss or inhibition triggers cytosolic DNA accumulation and cGAS-STING signaling activation, leading to enhanced immune response in PRMT6-deficient colon tumors or xenografts. Pharmacological inhibition of PRMT6 using EPZ020411 promotes mutagenesis and destabilizes MutSα or MutSβ assembly, and prolonged EPZ020411 exposure maintains an MSI-like phenotype in microsatellite stability (MSS) cells. EPZ020411 treatment sensitizes ICB efficacy of MSS cells, but not MSI cells in vivo. Similar effects have been observed in MSS colon tumors induced by AOM/DSS.

Conclusions Our study provides a preclinical proof of concept to overcome resistance to immunotherapy by targeting PRMT6 in CRC with MSS.

INTRODUCTION

Colorectal cancer (CRC) is the third most common cancer type and the second-leading

WHAT IS ALREADY KNOWN ON THIS TOPIC

⇒ While colorectal cancer (CRC) patients with deficient mismatch repair (MMR) benefit from immune checkpoint blockade (ICB) therapy, those with MMR-proficient tumors demonstrate limited therapeutic response. Given that MMR status controls sensitivity to ICB, this study investigates whether modulating MMR functionality can enhance the efficacy of ICB treatment in MMR proficient CRC.

WHAT THIS STUDY ADDS

⇒ This study demonstrates that PRMT6 is a critical regulator of MMR activity via MSH2 methylation and MutSα or MutSβ complex assembly. Pharmacological inhibition or PRMT6 loss promotes mutagenesis and sensitizes ICB efficacy of MMR tumors in preclinical models.

HOW THIS STUDY MIGHT AFFECT RESEARCH, PRACTICE OR POLICY

⇒ Our study highlights the critical determinant of PRMT6 in ICB efficacy in MMR proficient CRC, and our study provides a preclinical proof of concept to overcome resistance to immunotherapy by targeting PRMT6 in CRC with microsatellite stability.

cause of cancer deaths worldwide. An estimated annual 1.8million new cases were reported, which may increase to 2.5million in 2035.¹ Although early detection through screening, surgical procedures, and advances in primary and adjuvant treatments have greatly improved the prognosis of patients with CRC, 25% of CRC patients are diagnosed at an advanced stage, compromising therapeutic options.² Over the past decade, the clinical approval and application of immunotherapy via immune-checkpoint blockade (ICB) has achieved great success in several tumor types, rapidly revolutionizing the paradigm of cancer treatment and our current understanding of cancer biology.^{3,4} However, only a subset of patients benefits from ICB

therapy, with a range of 10%–30% in different cancer types. Several parameters have been identified that could predict patients who are most likely to respond to immunotherapy, including tumor mutational burden, microsatellite instability (MSI), PD-L1 expression level, and IFN γ signaling.⁵ In CRC, ICB therapy (anti-PD1 antibody) was approved in 2017 for the treatment of tumors with deficient mismatch repair (dMMR) or MSI-high (MSI-H).^{6–8} However, less than 5% of patients with metastatic CRC are dMMR or MSI-H and benefit from anti-PD-1 treatment.^{6,9,10} Because of low neoantigen levels and immune cell infiltration,^{11,12} MMR-proficient tumors show limited response to ICB therapy. It is a challenging yet critical issue to determine how to make CRC patients with MMR-proficient tumors benefit from immunotherapy.

CRC with dMMR-MSI-H signature has high overall mutation burden (>12 mutations per 10⁶ DNA bases) and prominent tumor-infiltrating lymphocytes, indicating that defects in MMR are critical for effective immune response and antitumor efficacy.^{13–15} MMR corrects DNA mismatches generated during DNA replication and is one of the most important guardians of genomic integrity, particularly microsatellite stability (MSS).¹⁶ Recognition and initiation of a mismatch are mediated by the mutS homologue MutS α or MutS β complex, in which MSH2 heterodimerizes with MSH6 or MSH3, respectively.¹⁷ MutS α are primarily responsible for repairing single base-base and insertion/deletion (ID) mismatches, and MutS β preferentially recognizes large ID mismatches.¹⁸ MutS α or MutS β initiates the recruitment of the heterodimer of mutL homologue 1 (MLH1) and postmeiotic segregation increased 2 (PMS2), which further recruits additional proteins in MMR, including proliferation-cell-nuclear antigen (PCNA), replication factor C (RFC), exonuclease 1 (EXO1), replication protein A (RPA), and DNA ligase I (LIG1).¹⁹ MMR deficiency is caused by mutations or deletions of either MLH1, MSH2, MSH6, and/or PMS2 or MLH1 promoter methylation.²⁰ Given the predictive value of dMMR resulting in MSI for response to PD-1 blockade, we reasoned whether targeting the MMR-proficient system in MSS tumors might lead to the creation of neoepitopes that boost the immune response. However, inhibitors targeting MMR component(s) have not yet been reported.

It has been well established that post-translational modifications (PTMs) control all aspects of protein function.^{21,22} Therefore, identifying key PTMs of MMR components might offer novel therapeutic targets for monitoring MMR activity. As MutS α or MutS β complex share MSH2 in common, MSH2 might be a suitable option that could be targeted for dual inhibition of both MutS α and MutS β . PTM of MSH2 has been reported in several studies. Early investigation showed that protein kinase C (PKC) phosphorylates both MSH2 and MSH6, an event required for nuclear translocation and increased mismatch binding capacity of MutS α .²³ However, the specific phosphorylation site(s) have not been identified. MSH2 is also phosphorylated by NPM-ALK at tyrosine

238 by oncogenic fusion protein NPM-ALK, leading to impaired MMR in anaplastic large cell lymphoma.²⁴ Histone deacetylase 6 (HDAC6) and HDAC10 were found to separately deacetylate MSH2 at distinct sites of its C-terminus and N-terminus, which increases MSH2 ubiquitination and degradation and ultimately reduces DNA MMR activities.^{25,26} Conversely, ubiquitin-specific peptidase 10 (USP10) deubiquitinates MSH2 and compromises DNA damage response and MMR activity.²⁷

Protein arginine methyltransferases (PRMTs) are a family of enzymes that catalyze protein arginine methylation. PRMTs are classified into three types: type I PRMTs (PRMT1, 2, 3, 4, 6, and 8) generate monomethyl arginine (MMA) and asymmetric dimethyl arginine (ADMA); type II PRMTs (PRMT5 and 9) produce MMA and symmetric dimethyl arginine, and PRMT7 belongs to type III and functions only as an MMA methyltransferase. PRMTs play diverse roles in many cellular processes, including gene transcription, RNA splicing, DNA damage repair, and cell cycle progression and immune response. PRMT6 is a type I PRMT implicated in cell cycle arrest, mRNA alternative splicing, mitosis, and cancer stemness via methylating multiple substrates.^{28–32}

In this study, we have identified that PRMT6 is a novel regulator of MMR activity through dimethylating MSH2. Such a modification significantly promotes MutS α or MutS β complex assembly and MMR capacity. Targeting PRMT6 using its inhibitor EPZ020411 in MMR-proficient CRC cells induces an MSI-like phenotype that shows sensitivity to immunotherapy. Therefore, our study provides a preclinical proof of concept to overcome resistance to immunotherapy by targeting PRMT6 in CRC.

MATERIAL AND METHODS

Reagents and antibodies

DMEM high-glucose and RPMI 1640 medium were purchased from Shanghai BasalMedia Technologies (China). EPZ020411 (HY-12970A) and 6-Thioguanine (6-TG, HY-13765) were obtained from MedChemExpress, Shanghai, China. Pico488 (Cat# 12,010) was purchased from Lumiprobe. Annexin V-FITC Apoptosis Detection Kit (40302ES20), GST Agarose Resin (20507ES10), Ni-NTA Agarose Resin (20502ES10) were purchased from Yeasen Biotechnology Shanghai, China. Antibodies used for immunoblot against MSH2 (15520-1-AP, 1:1000), MSH3 (22393-1-AP, 1:1000), MSH6 (18120-1-AP, 1:1000), PRMT6 (15395-1-AP, 1:1000), and GAPDH (60004-1-Ig, 1:5000), IRF3 (11312-1-AP, 1:1000) were purchased from Proteintech (Wuhan, China). Phospho-IRF-3 (Ser386, 37829S, 1:1000), Phospho-STAT1 (Tyr701, 9167S, 1:1000), and STAT1 (14994S, 1:1000) were purchased from Cell Signaling Technology. FLAG M2 gel (A2220) and mouse anti-FLAG antibody were obtained from Sigma-Aldrich (USA). Antibodies for FACS analysis: CD86 (PE-Cy7, Clone: GL1, BD Pharmingen, Cat: 560582), CD206 (Brilliant Violet 421, Clone: C068C2, BioLegend, Cat:141717), NK1.1 (PE,

Clone: PK136, BioLegend, Cat: 108707), CD8a (PerCP-Cy 5.5, Clone: 53-6.7, BD Pharmingen, Cat: 551162), CD11b (FITC, Clone: M1/70, BD Pharmingen, Cat: 557396), F4/80 (APC-R700, Clone: T45-2342, BD Horizon, Cat: 565787), CD45 (BV510, Clone: 30-F11, BD Horizon, Cat: 563891), CD3 ϵ (FITC, Clone: 145-2C11, BioLegend, Cat: 100306), CD4 (BV605, Clone: RM4-5, BD Horizon, Cat: 563151), Ly-6C (PE, Clone: AL-21, BD Pharmingen, Cat: 560592), Ly-6G (APC, Clone: 1A8, BD Pharmingen, Cat: 560599), and Mouse BD Fc Block (Purified, Clone: 2.4G2, BD Pharmingen, Cat: 553141).

Cell culture and lentivirus preparation

Human Embryonic Kidney (HEK) 293T, SW480, SW620, HT29, HCT116, MC38, and CT26 cells were purchased from the Cell Bank of Shanghai Institutes of Biological Sciences. SW480, SW620, HT29, and HCT116 cells were maintained in RPMI 1640 medium, and HEK-293T, MC38, and CT26 cells were maintained in DMEM high-glucose medium with 10% FBS. All cell lines underwent detection for mycoplasma contaminants using a Mycoplasma Detection Kit (40611ES25, YEASEN, Shanghai, China) and were confirmed to be mycoplasma-negative. STR authentication was performed to confirm the identity. Lentivirus was prepared as previously described.³³

Preparation of knockdown and knockout cell lines

PRMT6 or MSH2 knockout in SW480 cell lines were generated by CRISPR-Cas9 technologies using sgRNA sequences targeting PRMT6 (sg1: TGCTGCTGCGC-TACAAAGT; sg2: ACTTTGTAGCGCAGCAGCAC; sg3: CCCATCCACTCGCTCACGA; sg4: TCGTGAGCGAGT-GGATGGGC) or MSH2 (sg1: TCAGCTTCCATTGGT-GTTG). Positive single clones for PRMT6 deficiency were confirmed by immunoblot. For MSH2, SW480 cells or PRMT6-depleted cells were infected with sgMSH2 lentivirus, and MSH2 depletion was verified by immunoblot. PRMT6 knockdown in human CRC cells or mouse CT26 cells was achieved by RNA interference using short interfering RNA (siRNA) and lentiviral vector-based Short Hairpin RNA (shRNA) (shPRMT6-1: CACGGACGTTTC AGGAGAGAT; shPRMT6-2: CACCGGCATTCTGAGC ATCTT or shPrmt6: CGCATACTTCTGCGCTACAAA).

Generation of *Prmt6*^{-/-} mice

Prmt6^{-/-} mice were constructed by the CRISPR-Cas9 system as previously described. Briefly, a mixture of Cas9 mRNA and two sgRNAs was injected into the fertilized eggs, which were then transferred into C57BL/6N female mice to yield F0 generation mice. F1 generation mice were prepared by mating F0 mice with wild-type littermates. The genotypes of *Prmt6*^{-/-} mice were confirmed by PCR amplification using genomic DNA from tails. The following primers: 5'-AGCTGTACTACGAGTGCT-3' and 5'-CATCCACTCGCTGACGA-3' were used for PCR amplification and sequencing. All mice were maintained in specific pathogen-free facilities.

Azoxymethane/dextran sodium sulfate-induced CRC model and treatments

Eight-week-old C57BL/6 mice were injected intraperitoneally with azoxymethane (AOM) (10 mg/kg in PBS). One week later, mice were given 2.5% dextran sodium sulfate (DSS) in the drinking water for 3–5 days, and an additional 2 weeks was followed with normal drinking water. This procedure was repeated three times. Two additional months were required after DSS challenge before mice were sacrificed for subsequent analysis. For drug treatment, mice were given vehicle or EPZ020411 (10 mg/kg) intraperitoneally once a day for 5 weeks at the end of DSS challenge. Anti-PD1 antibody was given every 3 days through intraperitoneal injections at doses of 200 μ g per mouse for 5 weeks. For combination therapy, mice were administered with equal EPZ020411 and anti-PD1 antibody. An additional 1 month was required after treatment before mice were sacrificed for subsequent analysis.

Subcutaneous xenograft model and treatments

For the subcutaneous xenograft model, 5×10^4 CT26 or MC38 cells suspended in 100 μ L PBS were injected subcutaneously into 5-week-old C57BL/6 or BALB/c mice (5–6 mice per group). Three weeks later, tumor weight was examined, calculated, and collected for subsequent histological analysis. For drug treatment, mice were given vehicle or EPZ020411 (10 mg/kg) intraperitoneally after tumor inoculation once a day for 3 weeks. Anti-PD1 antibody was given every 3 days through intraperitoneal injections at doses of 200 μ g per mouse for 3 weeks. For combination therapy, mice were administered with equal EPZ020411 and anti-PD1 antibody.

For survival analysis, mice were monitored for signs of distress, such as weakness and weight loss, which resulted in mice being killed. Mouse survival was analyzed using the Kaplan-Meier method.

CRC organoid establishment and culture

Fresh CRC tumors from *Prmt6*^{-/-} and littermate mice were minced into small pieces and digested with collagenase IV (400 U/mL, Sigma) and DNase I (100 μ g/mL, Yeasen) in FBS-free RPMI 1640 medium for 30–45 min at 37°C. The single cells were depleted of erythrocytes by hypotonic lysis and counted using the Automatic Cell Counter Countess 3. A 25 μ L cell suspension with 25 μ L Matrigel containing 1×10^4 cells was plated in a prewarmed 24-well plate. 20 min later, 500 μ L expansion medium (1 \times B-27 supplement, 10 μ g/mL R-spondin, 10 μ g/mL Noggin, 1.25 mM N-acetylcysteine, 10 mM nicotinamide, 0.5 nM A83-01, 5 μ M Y-27632, 0.5 μ M SB202190, 1 \times N2 supplement, 50 ng/mL epidermal growth factor in DMEM/F12 medium) was added. Organoids were photographed using microscopy every day.

FACS analysis

Xenografts or colon tumor tissues were cut into small pieces and digested with collagenase IV (400 U/mL,

Sigma) and DNase I (100 µg/mL, Yeasen) in FBS-free RPMI 1640 medium for 30–45 min at 37°C. The resulting mixture was filtered through 40 µm cell strainers to obtain single-cell suspensions. The single cells were depleted of erythrocytes by hypotonic lysis. Approximately 1×10^6 single cells were blocked with FcR Blocking Reagent for 15 min and incubated with indicated antibodies for 20 min at 4°C. Cells were washed twice with PBS and resuspended in 200 µL PBS for sample analysis using Flow cytometry. For intracellular staining (CD86 and CD206), cells were incubated with Fixation/Permeabilization working solution (BD) for 30 min, washed twice with working solution of Perm/Wash buffer, and incubated with anti-CD86 and anti-CD206 antibodies for 30 min. Cells were then washed twice and resuspended in 200 µL working solution of Perm/Wash buffer for subsequent analysis. For analysis of cell apoptosis, SW480 cells were treated with CDDP (5 µM) for 48 hours and subjected to FACS analysis using Annexin V-FITC Apoptosis Detection Kit (YEASEN, 40302ES20).

HE and immunohistochemistry staining

Formalin-fixed and paraffin-embedded xenografts or CRC tumors were analyzed by HE or immunohistochemistry (IHC) as previously reported.^{33 34} The antibodies used for IHC were: Ki-67 (Proteintech, 27309-1-AP, 1:5000), anti-CD8 (GB15068, Servicebio, China) and PRMT6 (Proteintech, 15395-1-AP, 1:100). IHC scoring of PRMT6 in CRC samples was evaluated as previously reported.³⁴ Briefly, the staining intensity was graded from 0 to 2 (0, no staining; 1, weak; 2, strong). The staining extent was graded from 0 to 4 based on the percentage of immunoreactive tumor cells (0%, 1%–5%, 6%–25%, 26%–75%, 76%–100%). A score ranging from 0 to 8 was calculated by multiplying the staining extent score with the staining intensity score.

HPRT mutability assay

Cells (2×10^5) were seeded in triplicate in 6-well plates containing 5 µM 6-thioguanine (6-TG). 5×10^2 cells were seeded in 6-well plates without 6-TG treatment to determine the plating efficiency. 2–3 weeks later, the colonies were fixed and stained with 0.5% crystal violet, and the mutation frequency was calculated as previously reported.^{35 36}

Colony formation assay and drug response

1×10^4 cells were seeded into 6-well plates and were cultured in medium containing the indicated dose of EPZ020411 for 14 days. Cells were then fixed with 4% formaldehyde in PBS and stained with 0.5% crystal violet. Crystal violet was eluted using 33% acetic acid and quantified by measuring the absorbance at 590 nm with a plate reader.

MMR reporter system

The MMR reporter vector pCAR-OF (out-of-frame) was prepared as previously described with minor modification.³⁷ The GFP gene preceded by a 58 bp out-of-frame CA

repeat region was inserted into the pLenti vector, which will not generate GFP signal unless a frame-restoring mutation occurs. The pCAR-IF (In-frame) was used as a control, which contains a 57 bp CA repeat region resulting in GFP expression. For MMR reporter activity evaluation, cells were coinfecting with pCAR-OF and plenti-CMV-mCherry, and 5–6 days postinfection, cells were detached for analysis using FACS. MMR reporter activity was calculated by the percentage of the number of GFP-positive cells relative to mCherry-positive cells after correction.

Microscopy and immunofluorescence analysis

To detect cytosolic DNA, indicated cells were fixed and incubated with PicoGreen reagent for 2 hours, and washed with PBS five times before mounting with DAPI and imaging via Leica TCS SP8 confocal microscope.

In vitro methylation assay

A 2 µg of recombinant GST-MSH2 purified from *Escherichia coli* was incubated with 2 µg FLAG-PRMT6 purified from HEK-293T cells in the methylation buffer (50 mM Tris pH 8.5, 20 mM KCl, 10 mM MgCl₂, 1 mM β-mercaptoethanol, 100 mM sucrose and 0.1 mM adenosyl-L-methionine) at 30°C for 30 min. The reaction was stopped by adding 5×SDS loading buffer and was separated by SDS-PAGE. The protein band corresponding to GST-MSH2 was cut into pieces, followed by destaining, in-gel trypsin digestion, peptide extraction, liquid chromatography coupled to tandem mass spectrometry (LC-MS/MS) analysis, and protein methylation identification as previously described.^{33 34}

Identification of MSH2 interacting proteins and methylation

HT29 cells infected with vector or FLAG-MSH2 lentivirus were lysed by RIPA buffer (50 mM Tris (pH 7.4), 250 mM NaCl, 2% NP-40, 1% sodium deoxycholate, 1 mM EDTA and 20% glycerol) supplemented with protease inhibitor and phosphatase inhibitors, and the supernatant was incubated with 40 µL FLAG-M2 gel overnight on a gentle rotating machine. The resulting pellet was washed five times with RIPA buffer and then eluted with 500 µL FLAG peptide (5 mg/mL) in TBS (10 mM Tris HCL, 150 mM NaCl, pH7.4). The eluates were recovered using ultrafiltration spin columns (3 kDa), and were subjected to SDS-PAGE and Coomassie blue staining. Protein band cutting, in-gel trypsin digestion, peptide extraction, LC-MS/MS analysis, and protein identification were performed as previously described.^{33 34}

Immunoblot and immunoprecipitation analyses

Cells were rinsed with PBS and lysed with RIPA buffer supplemented with protease inhibitor and phosphatase inhibitors (MedChemExpress, Shanghai, China). The cell lysates were quantified by BCA Protein Quantification Kit (E112-01, Vazyme), resolved by SDS-PAGE, and immunoblotted with the indicated antibodies. For immunoprecipitation, the cell lysates were incubated with 15 µL FLAG-M2 gel overnight on a gentle rotating machine, and the immunoprecipitates were washed five times with

RIPA buffer before SDS-PAGE separation and immunoblot analysis with indicated antibodies.

Statistical analysis

All quantitative data are presented as the mean \pm SD of three biologically independent experiments or samples. Statistical analyses were performed using GraphPad Prism V.10.1, and significance was determined by two-tailed Student's t-test. The comparisons among three or more groups were first performed by the one-way analysis of variance test if the variation between groups was comparable. Overall survival was evaluated by the Kaplan-Meier survival curve and the log-rank test using GraphPad Prism V.10.1. A $p < 0.05$ was considered significant.

RESULT

PRMT6 binds to MSH2

To profile its PTMs, FLAG-tagged MSH2 was expressed in HT29, an MSS-proficient CRC cell line. Purified MSH2 protein was analyzed by LC-MS/MS. Interestingly, MSH2 was monomethylated or demethylated at multiple sites (including arginine and lysine residues), in addition to the phosphorylation and acetylation events as previously reported.^{23–27} Given that most lysine methyltransferases are large proteins and are not amenable to gene manipulation, we, therefore, focused on the methylation at arginine residues. To this end, five potential sites were identified (figure 1A). Co-immunoprecipitation (Co-IP) and LC-MS/MS were performed to identify the potential PRMTs (figure 1B). PRMT6 was identified and confirmed as a novel MSH2 interacting partner (figure 1C). The interaction between MSH2 and PRMT6 was direct, as evidenced by His pulldown using his-PRMT6 and GST-MSH2 (figure 1D). To figure out whether the observed interaction was related to MSH2 methylation, a catalytic methyltransferase inactive mutant PRMT6 (termed as PRMT6-mu) was prepared. Indeed, compared with wild-type PRMT6, PRMT6-mu significantly abolished its binding to MSH2 (figure 1E). Moreover, deletion of the methyltransferase domain of PRMT6 diminished MSH2/PRMT6 interaction (figure 1F). To determine the region(s) mediating the interaction, several fragments encoding various domains of MSH2 were prepared and were evaluated individually for the interaction with PRMT6. The region spanning from aa 297–378 (aa, amino acid) of MSH2 was likely for the interaction with PRMT6 (figure 1G). Collectively, PRMT6 directly interacts with MSH2.

PRMT6 methylates MSH2 and regulates MMR activity

To test whether PRMT6 is implicated in MSH2 methylation, we determined the methylation levels of MSH2 with or without PRMT6 overexpression using an antibody that recognizes the asymmetric dimethyl arginine motif. Indeed, an increase of MSH2 methylation was observed following PRMT6 expression (figure 2A), an effect that was not seen in the presence of PRMT6-mu (figure 2B),

indicating the methylation event of MSH2 is related to an intact methyltransferase activity of PRMT6. In vitro methylation assays then were carried out to identify specific sites by which MSH2 is methylated by PRMT6. This led to the discovery of asymmetric demethylation at arginine 171 (R171) and 219 (R219) (figure 2C). Substitution of R171 and R219 with lysine individually impaired the methylation level of MSH2, and the double mutant (2RK) almost abolished its methylation (figure 2D). Next, we examine whether MSH2 methylation alters MSH2 function and activity. The protein stability of wild-type MSH2 or MSH2-2RK was comparable in cells treated with Cycloheximide (CHX), a translation inhibitor (data not shown), indicating that such a modification did not affect its protein turnover. By generating an MMR reporter system using the pLenti vector containing a GFP gene preceded by a 58bp CA repeat region (CA29), which is out of frame as previously described,³⁷ we found that PRMT6 deletion greatly decreased MMR activity, indicating that PRMT6 positively regulates MMR capacity (figure 2E). While MSH2 overexpression induced a threefold increase of MMR activity compared with vector control, the ability of MSH2-2RK was considerably compromised (figure 2E), suggesting MSH2 methylation by PRMT6 enhances its function and MMR capacity. Given that the MutS α or MutS β formed by heterodimer of MSH2 with MSH6 or MSH3 is important for recognition and initiation of a MMR, we next ask whether MSH2 methylation alters MutS α or MutS β complex assembly. Expectedly, PRMT6 deficiency remarkably reduced the association of MSH2 with either MSH3 or MSH6 (figure 2F). Consistently, R171K or R219K mutation of MSH2 alone or the MSH2-2RK mutant disrupted MutS α or MutS β complex formation (figure 2G). These observations were also supported by the finding that PRMT6 depletion significantly increased mutation frequency in MMR-proficient SW480 and HT29 cells, but the mutation frequency remained unchanged in MMR-deficient DLD-1 cells (figure 2H,I). In addition, the PRMT6/MSH2 binding was markedly increased in HEK-293T cells treated with various genotoxins associated with DNA damage and MMR repair, including CDDP (cis-diamminedichloroplatinum), 6-TG (6-thioguanine) and MNNG (N-methyl-N'-nitro-N-nitrosoguanidine) (online supplemental figure 1A). Indeed, PRMT6 deficiency rendered CRC cells sensitive to CDDP-mediated apoptosis (online supplemental figure 1B). Taken together, these data revealed that PRMT6 is a critical regulator of MMR via MSH2 methylation.

PRMT6 deletion prevents colon tumorigenesis in mice

Since the role of PRMT6 in MMR, we next ask how PRMT6 affects CRC progression. Analyses of PRMT6 expression in human mucosa and adenoma showed that PRMT6 was increased in adenoma tissues compared with normal mucosa (figure 3A). In line with this, PRMT6 is also elevated in human CRC tissues relative to normal counterparts, as revealed by IHC staining and grading

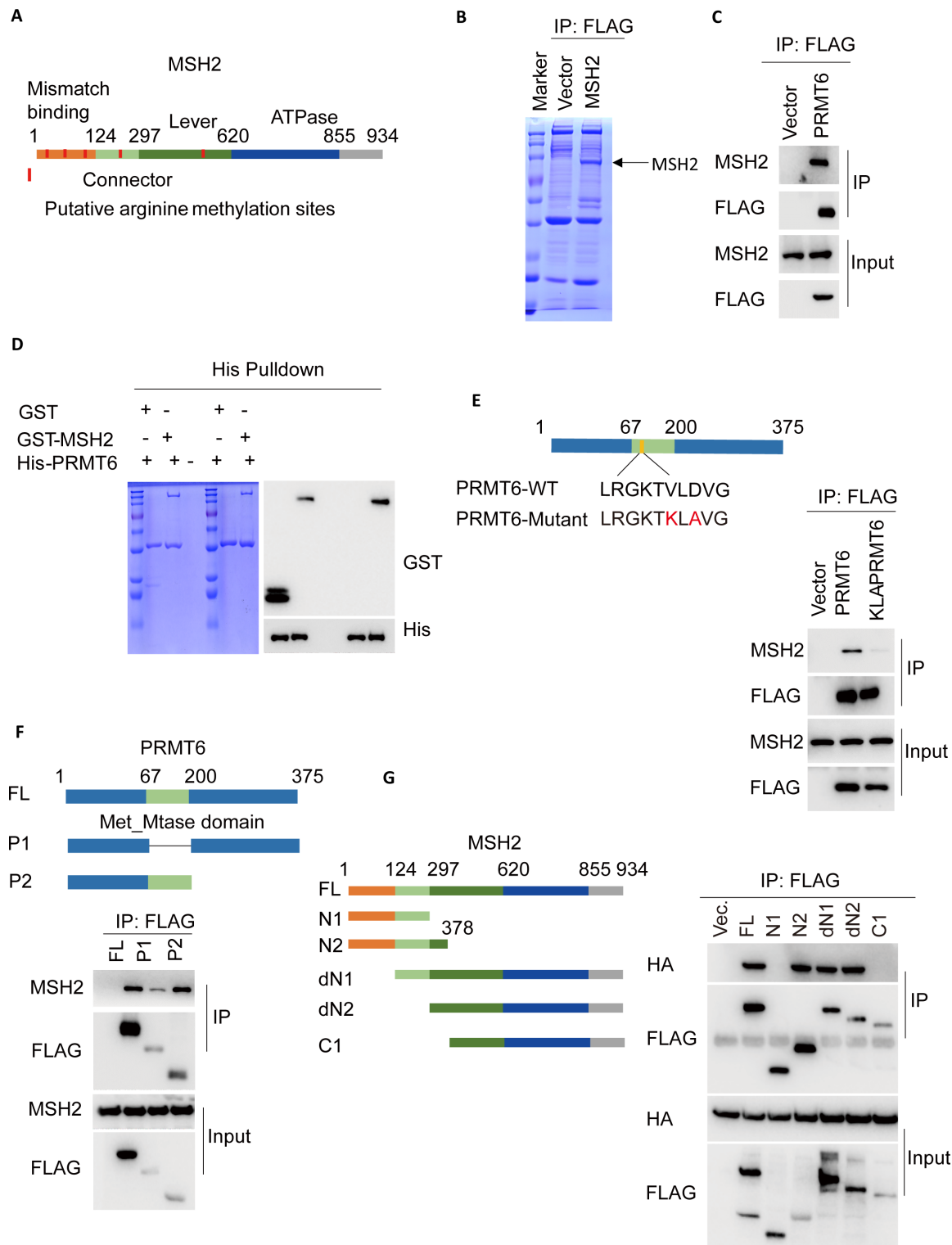


Figure 1 PRMT6 interacts with MSH2 directly. (A) Illustration of identified methylation sites in MSH2. Upper, the domain organization of MSH2. Potential methylation sites are shown. (B) Identification of MSH2 binding partners using IP/LC-MS/MS. Predicted MSH2 and PRMT6 were shown. (C) Association of MSH2/PRMT6 by IP and immunoblot. SW480 cells were infected with FLAG-PRMT6 or empty vector and subjected to immunoprecipitation using anti-Flag antibody. (D) Coomassie blue staining and immunoblot of GST-MSH2 incubated with his-PRMT6 after pulldown. (E) Immunoblot of MSH2 and FLAG-PRMT6 after co-immunoprecipitation. HEK-293T cells were transfected with empty vector, FLAG-PRMT6, or catalytic methyltransferase inactive mutant (PRMT6-mu) and subjected to immunoprecipitation using anti-Flag antibody. Upper, Schematic illustration of PRMT6 wild-type and PRMT6 catalytic inactive constructs. (F) Mapping of the region(s) of PRMT6 that interacts with MSH2. Upper, the domain organization of PRMT6 and the deletion constructs. (G) Mapping of the region(s) of MSH2 that interacts with PRMT6. Left, the deletion constructs of MSH2. LC-MS/MS, liquid chromatography coupled to tandem mass spectrometry; IP, immunoprecipitation.

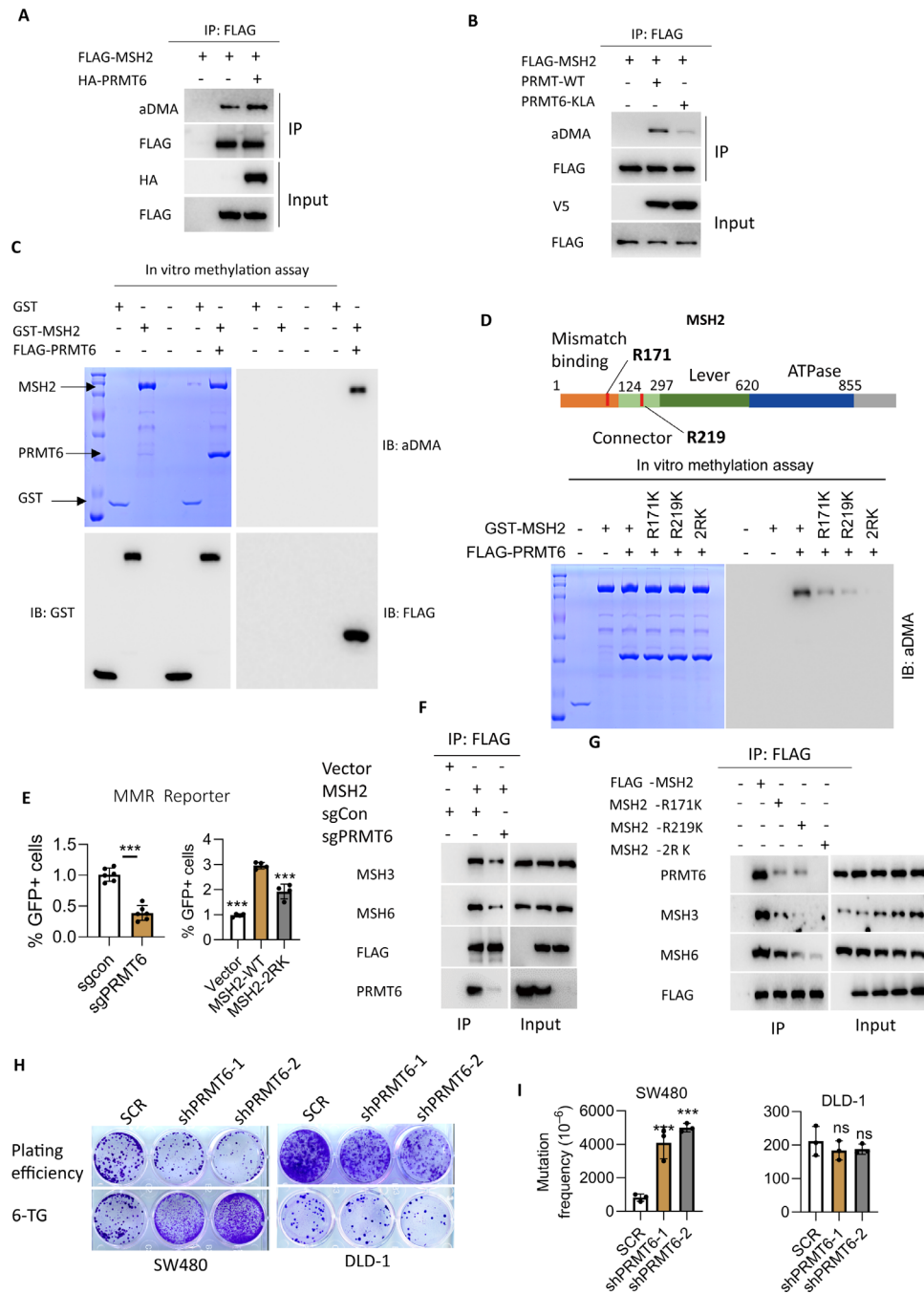


Figure 2 PRMT6 is methylated and is a regulator of MMR. (A) Immunoblot of MSH2 dimethylation after immunoprecipitation using anti-Flag antibody with or without PRMT6. (B) Determination of MSH2 di-methylation with vector, PRMT6, or PRMT6-mu by immunoblot after immunoprecipitation using anti-Flag antibody. (C) Examination of MSH2 dimethylation by immunoblot and Coomassie blue staining after in vitro methylation assay. Recombinant GST-MSH2 purified from *Escherichia coli* were incubated with FLAG-PRMT6 purified from HEK-293T cells in the methylation buffer for Coomassie blue staining, LC/MS-MS analysis, and immunoblot verification. (D) Illustration of identified methylation sites in MSH2. Examination of MSH2 di-methylation by immunoblot and Coomassie blue staining after in vitro methylation assay. Recombinant GST-MSH2, GST-MSH2-R171K, GST-MSH2-R219K, and GST-MSH2-2RK proteins purified from *Escherichia coli* were incubated with FLAG-PRMT6 purified from HEK-293T cells in the methylation buffer. (E) Evaluation of MMR reporter activity. Left, SW480 cells with or without PRMT6 were infected with pCAR-OF reporter and plenti-CMV-mCherry for FACS analysis. Right, 293 T cells were transfected with pCAR-OF reporter and plenti-CMV-mCherry with vector, MSH2-WT, and MSH2-2RK for FACS analysis. (F) Determination of MutS α and MutS β complex assembly with or without PRMT6 after immunoprecipitation using anti-Flag antibody. (G) Determination of MutS α and MutS β complex assembly in the presence of vector, FLAG-MSH2, FLAG-MSH2-R171K, FLAG-MSH2-R219K, and FLAG-MSH2-2RK after immunoprecipitation using anti-Flag antibody. (H) Representative images of HPRT mutability assay in SW480 and DLD-1 cells treated with 6-TG (5 μ M). (I) Mutation frequency of mutability assay. *P* values are determined by one-way ANOVA followed by Dunnett's multiple comparisons test. **p*<0.05, ***p*<0.01, ****p*<0.001. aDMA, Asymmetric Di-Methyl Arginine; MMR, mismatch repair.

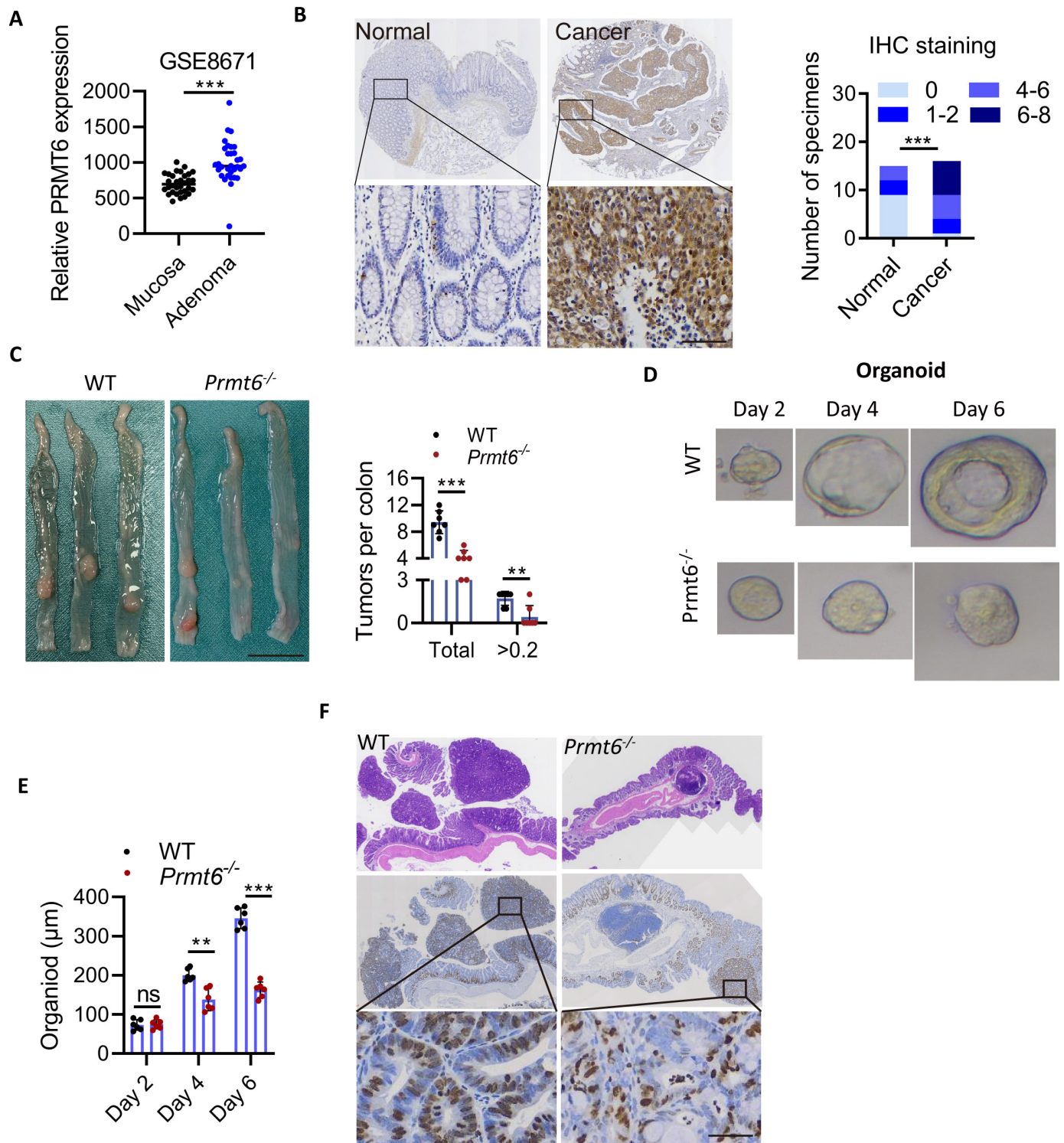


Figure 3 PRMT6 loss inhibits colon tumorigenesis in mice. (A) Analyses of PRMT6 expression in human mucosa and adenoma in the dataset of GSE8671. (B) Representative IHC images and statistical analysis of PRMT6 expression in normal and CRC tissues. Scale bar, 50 μm. (C) Gross images and statistical analysis of colon tumors in WT and *Prmt6*^{-/-} littermate mice (n=6). >0.2, diameter over 0.2 cm. (D) Representative images of organoid culture of colon tumors from indicated mice on indicated days. (E) Statistical analysis of organoid growth of colon tumors from indicated mice. (F) Histological analysis of tumor sections from indicated mice. Upper, HE staining of colon tumors. Lower, IHC staining of Ki-67 in colon tumors. Scale bar, 50 μm. Unpaired t test was used to determine statistical significance. *p<0.05, **p<0.01, ***p<0.001. CRC, colorectal cancer; IHC, immunohistochemistry.

(figure 3B). To determine its role in vivo, we generated PRMT6-deficient (*Prmt6*^{-/-}) mice using the CRISPR-Cas9 gene-editing system. No alterations were seen in *Prmt6*^{-/-} mice and the littermate mice in terms of body weight, colon length, and intestinal epithelial integrity (online supplemental figure 2A–C). In vivo tumorigenesis was then established in *Prmt6*^{-/-} mice and littermates using the AOM/DSS model. Consistently, *Prmt6*^{-/-} mice had less and smaller colon tumors than their wild-type littermates (figure 3C). Colon tumors collected from wild-type mice developed rapidly into organoids in ex vivo culture compared with those collected from *Prmt6*^{-/-} mice (figure 3D,E). Also, tumor burden was dramatically higher in wild-type littermates than *Prmt6*^{-/-} mice, which was consistent with the positive reactivity of Ki67, a proliferation marker (figure 3F).

Long-term exposure to PRMT6 inhibition induces an MSI-like phenotype

We next ask whether targeting PRMT6 suppresses CRC cell proliferation and MMR activity. Using a panel of MMR-proficient and MMR-deficient CRC cell lines, we found that the PRMT6 inhibitor EPZ020411 induced significant cell death within the 4 μM range, and the response to EPZ020411 between MMR-proficient and MMR-deficient CRC cell lines appeared to have no difference (figure 4A–C). To test its effect in vivo, CT26, a murine CRC cell line with MSS, was implanted in mice, receiving vehicle or EPZ020411. Consistently, tumor growth was suppressed in mice with EPZ020411 treatment (figure 4D). These results indicate that inhibition of PRMT6 is effective for CRC cells. Next, we determine whether acute PRMT6 inhibition (within 24 hours) affects MMR activity. Using an MMR-proficient cell line SW480, it was shown that both MutSα or MutSβ complex assembly was attenuated in SW480 cells in response to EPZ020411 treatment (figure 4E). As encouraged by this, we then determined whether long-term EPZ020411 incubation could induce an MSI-like phenotype in MSS CRC cells, such as CT26 and SW480. Given that the duration of drug delivery in most in vivo studies completes within 1 month, we, therefore, constructed a cellular model more relevant to in vivo study through challenging MSS CRC cells with EPZ020411 for 1 month. Unlike the effect in CT26 or SW480 with acute EPZ020411 treatment, CT26 or SW480 cells with prolonged exposure to EPZ020411 (termed as CT26T or SW480T thereafter) showed potent resistance to 6TG treatment (figure 4F), indicating an MSI-like phenotype and increased mutagenesis. In agreement with this observation, MMR capacity was significantly impaired in CT26T and SW480T cells (figure 4G). Importantly, the MSI-like phenotype persisted in CT26T cells with downregulation of MSH3 and attenuated MSH2/MSH3 or MSH2/MSH6 interaction (figure 4H). This might be due to the transcriptional repression of MMR-related genes, given that the similar effect was also observed in MSI CRC cells following acute EPZ020411 incubation (online supplemental figure 3A).

PRMT6 loss enhances antitumor immune response in CRC

Because we have demonstrated that PRMT6 inhibition induces an MSI-like phenotype in MSS CRC cells that might potentially boost antitumor immunity and ICB efficacy, we sought to test whether these findings can be exploited in in vivo studies. We first test this hypothesis in mice or xenografts with PRMT6 loss. Analyses of colon tumors derived from *Prmt6*^{-/-} mice and littermates revealed an increased infiltration of CD8⁺ cells, which was similar to the xenografts of CT26 with *Prmt6* depletion (figure 5A–C), indicating that PRMT6 loss potentially increases antitumor immune response. Multicolor flow cytometry further showed that the proportion of CD8⁺ cells and NK cells was increased greatly, while PMN-MDSC and M2 macrophage abundance was reduced in colon tumors derived from *Prmt6*^{-/-} mice compared with that of littermate mice (online supplemental figure 4 and figure 5D). Similarly, *Prmt6* depletion in CT26 induced an overall increase of CD45⁺ leukocytes, including the upregulation of CD4⁺ cells, CD8⁺ cells, and NK cells, and downregulation of PMN-MDSC (figure 5E). These findings demonstrated that PRMT6 loss is associated with a signature of active immune response in mice.

PRMT6 loss triggers cytosolic DNA release and the cGAS-STING pathway

Considering that MMR-deficient CRC sensitive to immunotherapy is due to neoantigen production and activation of the cGAS-STING pathway,^{38 39} we ask whether PRMT6-mediated MSH2 methylation and MMR activity are related to activation of the cGAS-STING pathway. To this end, we have performed RNA-sequencing (RNA-seq) analysis in SW480 cells with or without PRMT6 knockout to profile differentially expressed genes and signaling cascades (figure 6A). Indeed, interferon signaling and cytosolic DNA sensing pathway were significantly enriched in SW480 cells following PRMT6 loss or in CRC of TCGA datasets (figure 6B), indicating PRMT6 inhibits innate immune response in CRC. Some of the well-known genes of interferon and cytosolic DNA sensing pathway were significantly altered in PRMT6-deficient cells (figure 6C). Particularly, IFN regulatory factor 7 (IRF7) and IFN-stimulated gene 15 (ISG15), two critical factors that were induced in MMR-deficient cells,^{38 39} were dramatically upregulated in SW480 cells following PRMT6 loss (figure 6D). Consistently, PRMT6 loss or pharmacological inhibition in cells remarkably stimulated phosphorylation of STAT1 and IRF3 (figure 6E), indicating activated cGAS-STING pathway. To confirm whether the observed cGAS-STING pathway activation is due to the generation of cytosolic DNA, we measured cytosolic DNA using PicoGreen dye, a fluorescent stain that selectively binds to double-stranded DNA (dsDNA). Indeed, either PRMT6 loss or pharmacological inhibition of PRMT6 by EPZ020411 stimulated cytosolic DNA accumulation in SW480 cells indicative of the cytosolic DNA-activated cGAS-STING pathway (figure 6F,G). To further demonstrate whether PRMT6 deficiency induced cytosolic DNA

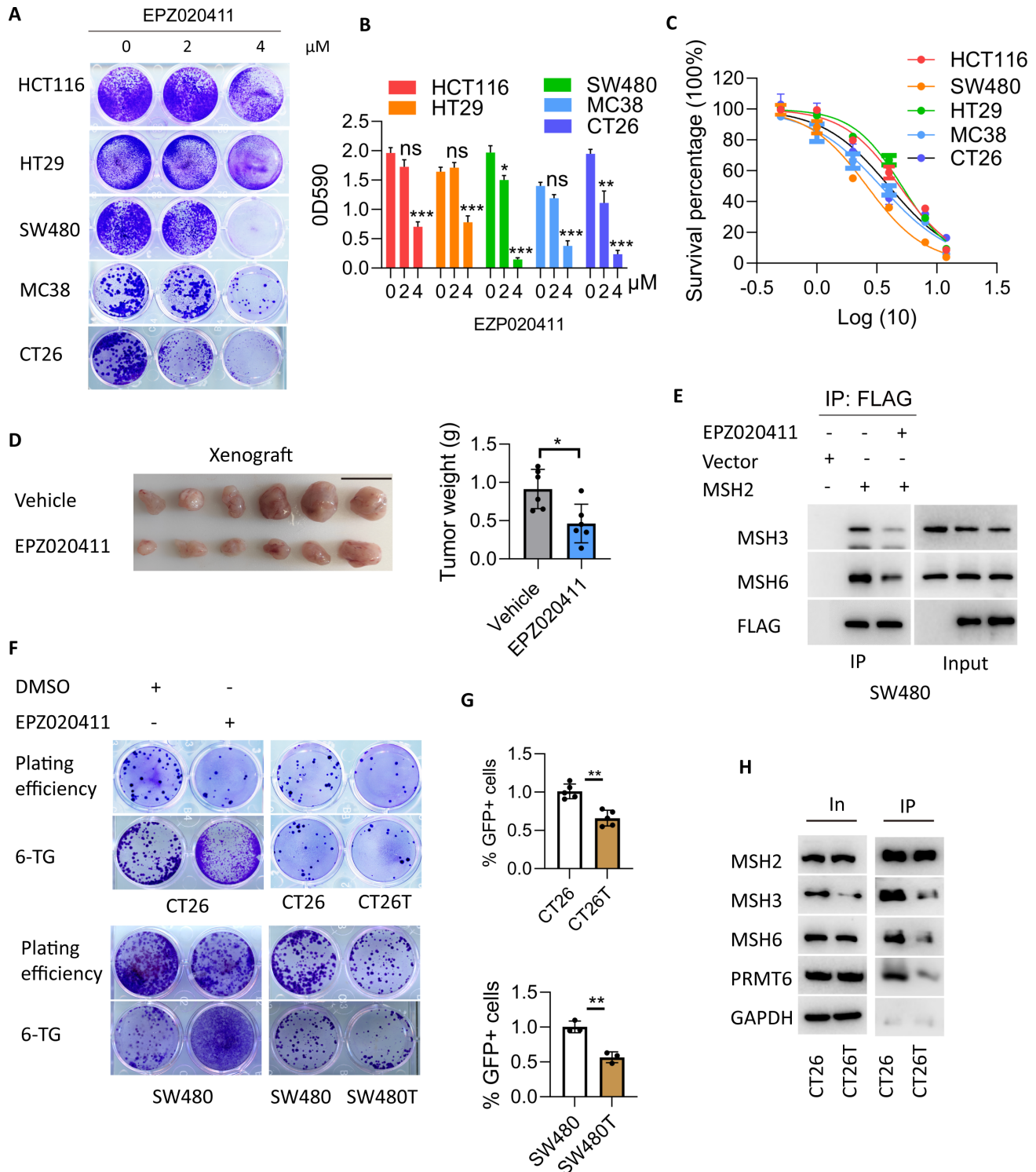


Figure 4 PRMT6 loss promotes mutagenesis and MSI phenotype. (A) Long-term colony formation assay of several CRC cell lines treated with the indicated dose of EPZ020411. (B) Quantification of cell death in indicated cells. Crystal violet was eluted using 33% acetic acid and quantified by measuring the absorbance at 590 nm with a plate reader. (C) EPZ020411 dose-response curves of CRC cells based on the CCK8 assay. (D) Images of xenografts treated with or without EPZ020411 (10 mg/kg) in BALB/c mice (n=6). Scale bar, 1 cm. (E) Quantification of tumor weight in mice with indicated treatment. (F) Determination of MSH2 binding to MSH3 or MSH6 in SW480 cells treated with or without EPZ020411 (4 μM for 24 hours). (G) Representative images of HPRT mutability assay in CT26 and SW480 cells. Left, CT26 and SW480 cells were treated with 6-TG (5 μM) with or without EPZ020411 (2 μM) for 2 weeks. Right, CT26 and SW480 cells were treated with EPZ020411 (4 μM) for 4 weeks, and the survived cells were termed as CT26 or SW480T. HPRT mutability assay was performed in CT26 and CT26T or SW480 and SW480T treated with 6-TG alone (4 μM). (H) Examination of MMR capacity in indicated cells. (I) Immunoblot of MMR proteins and MutS α and MutS β complex formation after immunoprecipitation using anti-MSH2 antibody. An unpaired t test was used to determine statistical significance. * $p<0.05$, ** $p<0.01$, *** $p<0.001$. MSI, microsatellite instability; MMR, mismatch repair.

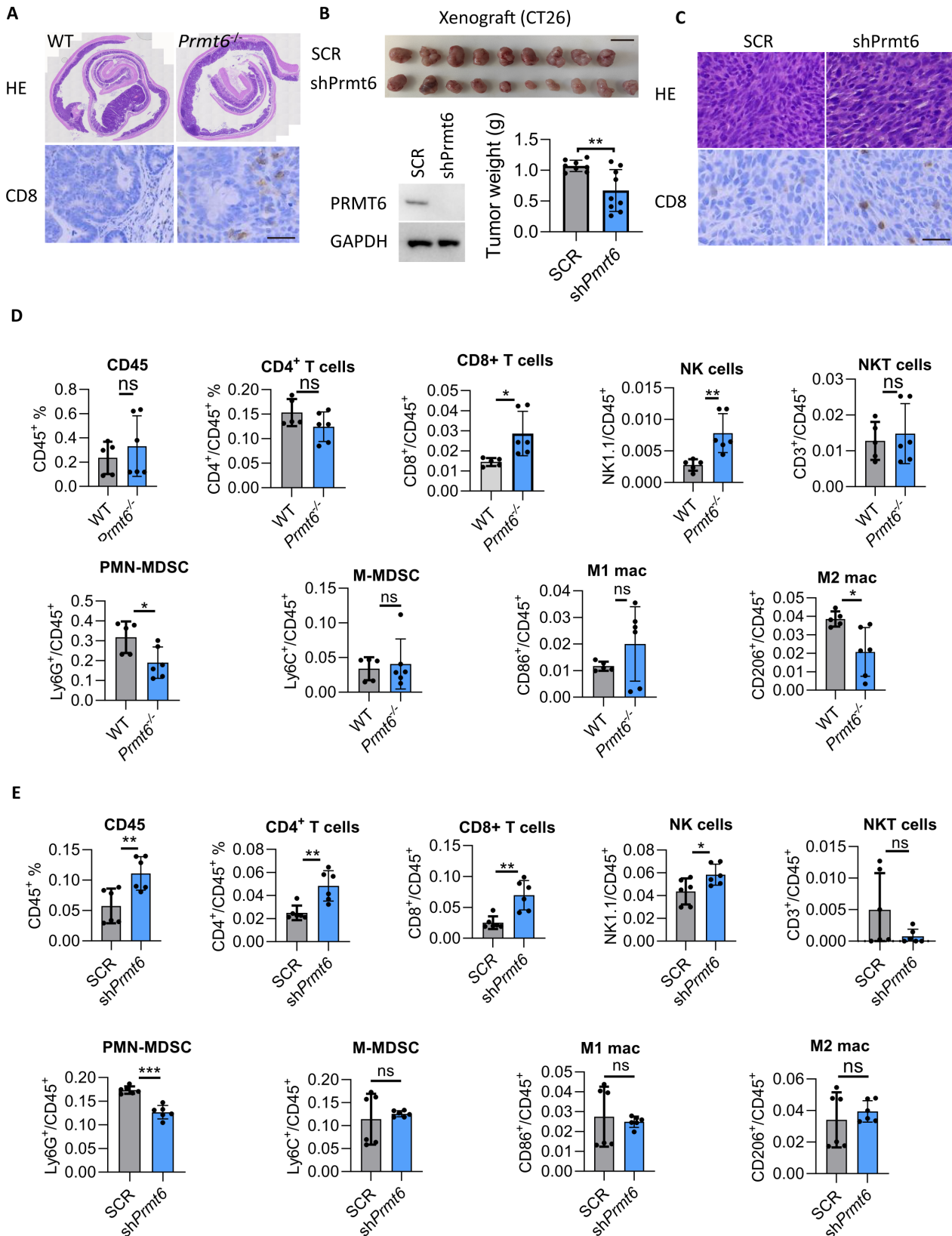


Figure 5 PRMT6 loss favors active immune response in mice. (A) Histological analysis of tumor sections from indicated mice. Upper, HE staining of colon tumors. Lower, IHC staining of CD8 in colon tumors. Scale bar, 40 μ m (B) *Prmt6* depletion inhibits CT26 cell proliferation in BALB/c mice. Upper, gross image of xenografts from indicated cells. Lower, determination of PRMT6 knockdown efficiency and quantification of tumor weight in indicated xenografts. Scale bar, 0.5 cm. (C) Histological analysis of tumor sections from indicated mice. Upper, HE staining of xenografts. Lower IHC staining of CD8 in xenografts. Representative flow cytometry analysis and quantification of indicated immune cell populations in colon tumors (D) and xenografts (E). n=6. Unpaired t test was used to determine statistical significance. *p<0.05, **p<0.01, ***p<0.001. IHC, immunohistochemistry.

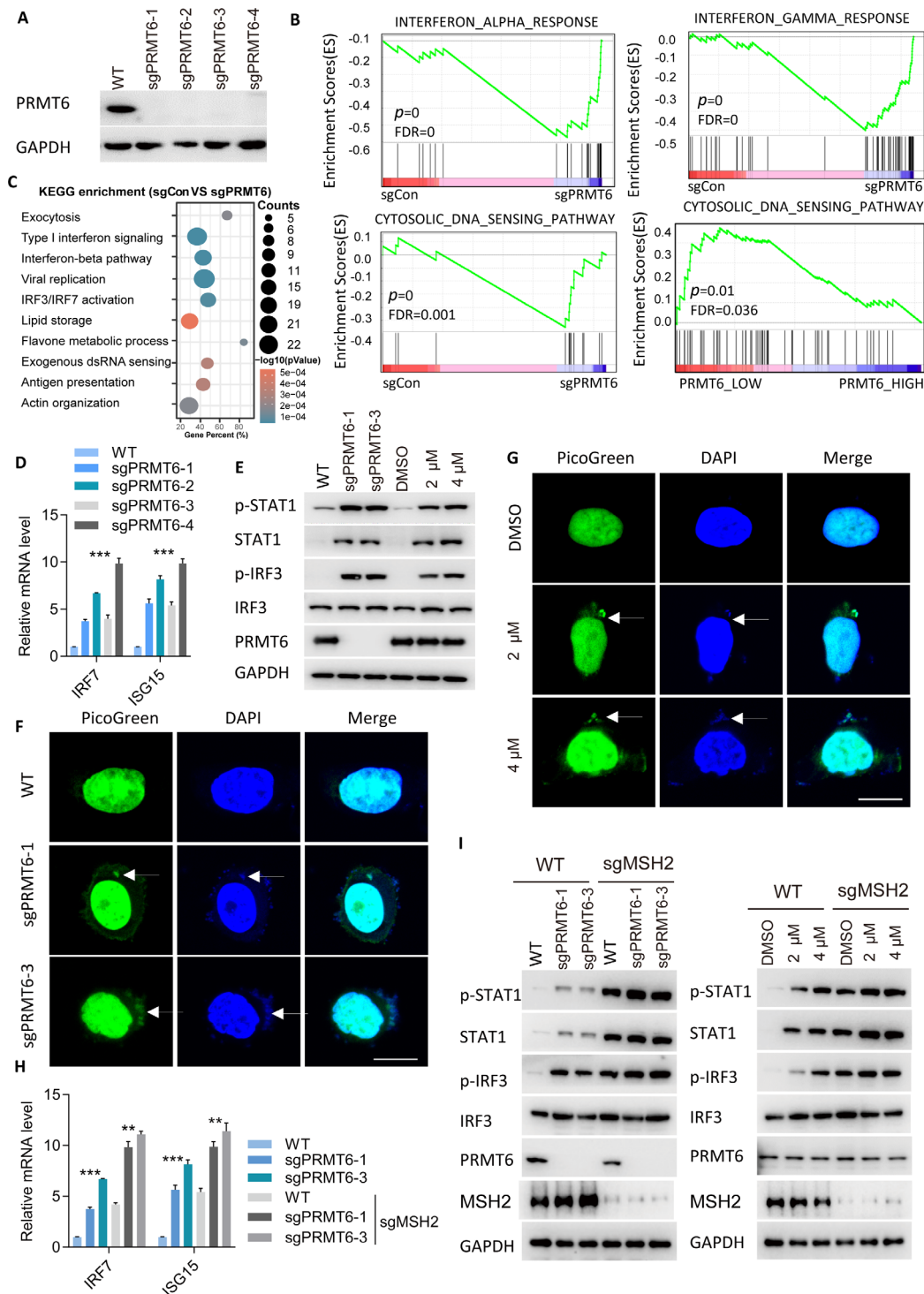


Figure 6 PRMT6 loss triggers cytosolic DNA accumulation and cGAS-STING signaling activation. (A) Generation and verification of PRMT6 knockout cell line in SW480. (B) Pathway enrichment of RNA-seq datasets in PRMT6-deleted cells or wild-type cells or TCGA datasets of patients with CRC stratified by median expression of PRMT6 expression as analyzed by GSEA (Gene Set Enrichment Analysis). (C) Heat-map demonstration of altered genes implicated in interferon signaling from RNA-seq dataset of PRMT6-deleted cells or wild-type cells. (D) Determination of IRT7 and ISG15 mRNA levels in PRMT6-deleted cells or wild-type cells by qPCR. (E) Immunoblot analysis of indicated protein levels in indicated cells with or without EPZ020411 treatment for 48 hours. (F) Detection of cytosolic DNA using PicoGreen staining in wild-type and PRMT6-deleted SW480 cells. DNA was detected using the PicoGreen fluorescence dye selectively binding dsDNA. Arrows point to cytosolic DNA. Scale bar, 15 μ m. (G) Detection of cytosolic DNA using PicoGreen staining in SW480 cells with or without EPZ020411 (4 μ M) treatment for 72 hours. Arrows point to cytosolic DNA. Scale bar, 15 μ m. (H) Determination of IRT7 and ISG15 mRNA levels in PRMT6-deleted cells or wild-type SW480 cells with or without MSH2 loss. (I) Immunoblot analysis of indicated protein levels in indicated cells (left) or indicated cells with or without EPZ020411 treatment for 48 hours. P values are determined by one-way ANOVA followed by Dunnett's multiple comparisons test. $*p<0.05$, $**p<0.01$, $***p<0.001$.

accumulation is linked to MMR defects via MSH2, we prepared MSH2 knockout in PRMT6-deleted SW480 cells and tested IRF7 and ISG15 expression and phosphorylation of STAT1 and IRF3. Not surprisingly, MSH2 depletion significantly attenuated the robust upregulation of IRF7 and ISG15 expression in cells with PRMT6 loss or inhibition (figure 6H). Similarly, phosphorylation of STAT1 and IRF3 was also impaired in PRMT6-deleted cells with further MSH2 loss (figure 6I). These results generally indicate that PRMT6 loss induced MMR defects and cytosolic DNA accumulation that activate the cGAS-STING pathway.

PRMT6 inhibition renders CRC cells sensitive to ICB

Since we have demonstrated that PRMT6 loss induced MMR defects that activate the cGAS-STING pathway and immune response, we next explore whether the induced-MSI phenotype would be maintained in CT26T cells that render them sensitive to ICB. CT26T cells were implanted in mice treated with vehicle, EPZ020411, PD1 antibody alone or in combination with EPZ020411, respectively. CT26T cells were slightly sensitive to EPZ020411, and a modest response was observed in mice with PD1 antibody treatment. However, CT26T cells with simultaneous treatment of EPZ020411 and PD1 showed dramatically enhanced response to PD1, as evidenced by reduced tumor weight, lower portion of Ki-67-positive cells, and increased CD8⁺ cell infiltration (figure 7A,B). This observation is further supported by FACS analysis showing an increased proportion of CD8⁺, NK cells, and M1 macrophages and reduced percentage of PMN-MDSC (figure 7C and online supplemental figure 5A). Importantly, combination therapy significantly extended the survival times of mice over either EPZ020411 or PD1 antibody alone (figure 7D). To rule out the potential off-target effect of EPZ020411, we test whether PRMT6 loss would also enhance ICB therapeutic efficacy. Indeed, PRMT6 depletion synergized with PD1, which efficiently suppressed CT26 xenograft progression, suggesting the on-target effect of EPZ020411 (online supplemental figure 5B,C). Although xenografts of pMMR MC38 cells showed a slight response to EPZ020411 treatment, the therapeutic efficacy of PD1 antibody was not further enhanced in combination with EPZ020411 (online supplemental figure 5D), indicating that PRMT6 facilitates ICB efficacy via modulating MMR capacity. Collectively, these data indicate that chronically treated cells maintained the MSI-like phenotype that showed increased sensitivity to PD-1 therapy. To further prove observed findings, the AOM/DSS was used to establish de novo CRC model, followed by EPZ020411, PD1 antibody alone or combined treatment. We found that either EPZ020411 or anti-PD-1 monotherapy alone slightly reduced the overall tumor number and size (figure 7E and online supplemental figure 5E). However, limited responses to either monotherapy were observed in tumors with a diameter of over 0.2 cm, which could be overcome by a combination therapy of EPZ020411 and anti-PD-1 (figure 7G). IHC staining of the tumor sections

confirmed significantly CD8⁺ infiltration in mice with combination therapy (figure 6G). Taken together, we have demonstrated that PRMT6 loss renders CRC sensitive to ICB in mice.

DISCUSSION

Studies with immunotherapy have revealed a subset of tumors harboring MMR deficiency (dMMR) that are sensitive to ICB, regardless of their tissue of origin.⁴⁰ However, dMMR is only detected in less than 5% of most cancer types, implying that most patients with cancers will not benefit from ICB therapy. It is meaningful to identify molecular determinants that control response to immunotherapy in pMMR patients for developing strategies to expand the clinical application of ICB therapy. Due to limited knowledge on how MMR is regulated, strategies targeting MMR are lacking. In this study, we have demonstrated that PRMT6 was a critical regulator of MMR capacity through dimethylation of MSH2, a shared component of MutS α or MutS β complex. PRMT6 belongs to type I PRMT, which generates MMA and aDMA. Notably, while PRMT6 loss significantly attenuated the MMR reporter activity, the MSH2 methylation-defective mutant only partially abolished the MMR activity compared with WT MSH2, indicating other mechanisms potentially involved in addition to its methylation by PRMT6. Possibly, other PRMTs or KMTs might be implicated in controlling MSH2 or other MMR proteins, thereby partially compensating for the loss of PRMT6 or defect in MSH2 methylation. This notion is supported in this study by the identification of multiple methylation sites at arginine and lysine residues of MSH2. Obviously, MSH2 and other MMR proteins are known to undergo various PTMs, including phosphorylation, acetylation, and ubiquitination, which can modulate their function, maintaining partial MMR activity. Future studies could explore the crosstalk between methylation and other PTMs and whether their inhibition further reduces MMR activity, which may provide further insights into the regulation of MMR. It is known that the MMR system is composed of multiple protein complexes that can partially compensate for each other's functions. For instance, the MutS α complex primarily recognizes base-base mismatches, while the MutS β complex is involved in detecting ID loops. It is possible that the residual MMR activity observed in the MSH2 methylation-defective mutant is mediated by the increased activity or stability of these alternative complexes, which will be interesting work for future study. Nevertheless, we have characterized a novel modification of MSH2 that controls MMR activity, at least partially.

To confirm whether the observed function of PRMT6 supports its role during colon tumorigenesis, we generated PRMT6-deficient mice. Expectedly, PRMT6-deficient mice had significantly fewer colon tumors than WT mice, which is consistent with elevated PRMT6 in patients with adenoma and colon cancers. We examined the MMR capacity with interest in colon tumors

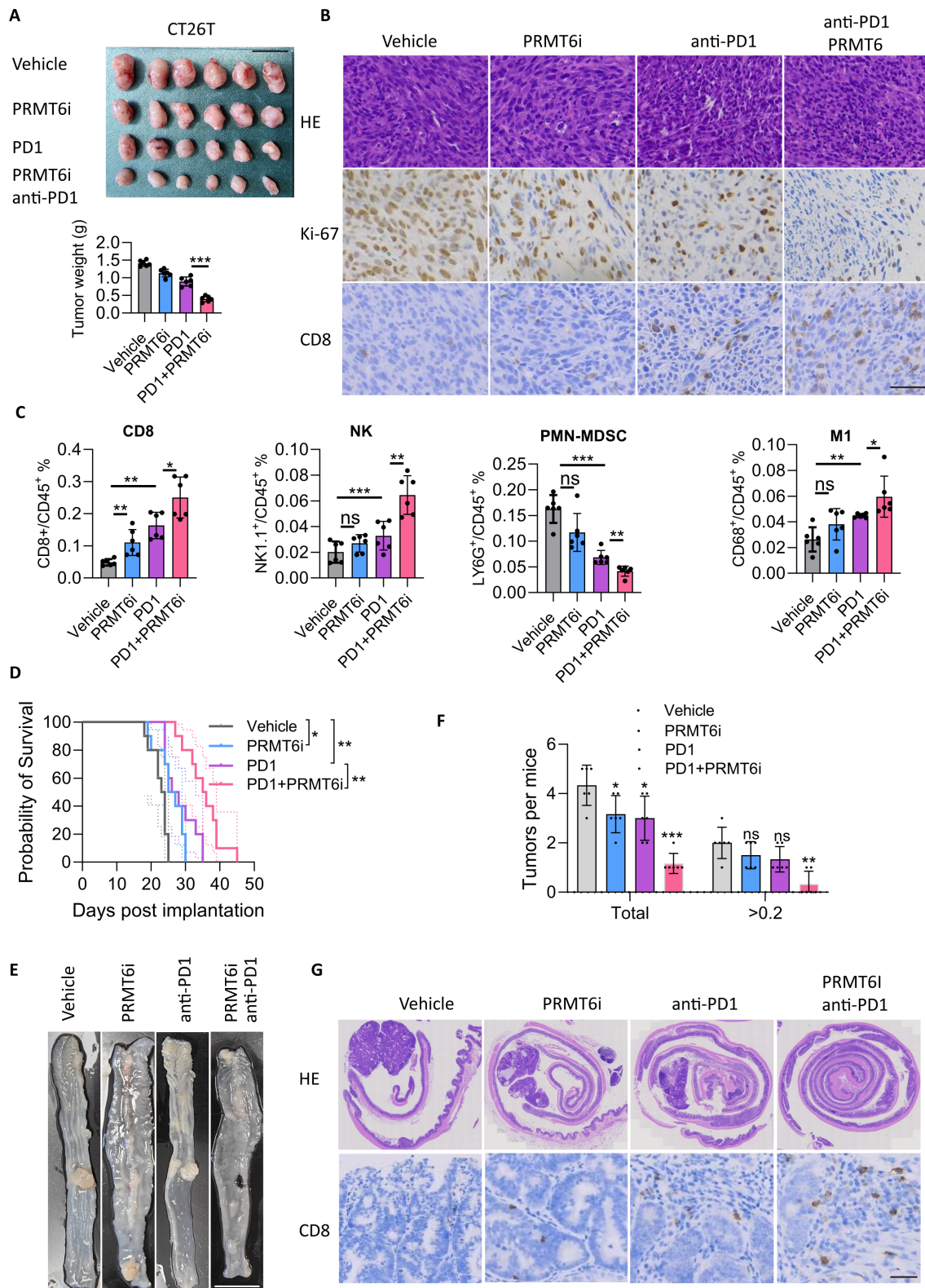


Figure 7 PRMT6 inhibition renders colon tumors sensitive to anti-PD1 therapy. (A) Gross image of indicated xenografts and quantification of tumor weight (n=6). Scale bar, 1 cm. (B) Histological analysis of tumor sections from indicated xenografts. Upper, HE staining of indicated tumor sections. Middle and lower, IHC staining of Ki-67 and CD8 in indicated tumor sections. Scale bar, 50 μ m. (C) Quantification of indicated immune cell populations in xenografts by FACS (n=6). (D) Survival analysis of indicated mice with indicated treatment (n=10). Gross images (E) and statistical analysis (F) of colon tumors in WT and *Prmt6*^{-/-} littermate mice (n=5). >0.2, diameter over 0.2 cm. Scale bar, 1 cm. (G) Histological analysis of tumor sections from indicated colon tumors. Upper, HE staining of indicated tumor sections. Lower, IHC staining of CD8 in indicated tumor sections. Scale bar, 30 μ m. P values were determined by one-way analysis of variance followed by Dunnett's multiple comparisons test. *p<0.05, **p<0.01, ***p<0.001. IHC, immunohistochemistry.

derived from PRMT6-deficient and WT mice. Although it is indeed consistent with *in vitro* results that PRMT6 loss prevented MutS α or MutS β complex assembly, an impaired MMR activity of colon cancer indicative of genomic instability in PRMT6-deficient mice appeared contradictory to reduced tumor growth. One hypothesis is that the AOM/DSS colon cancer model predominantly generates somatic mutations like APC, TP53, and KRAS that drive tumor progression. The genome instability caused by AOM/DSS treatments is independent from mutations of MMR pathways.⁴¹ Also, cell-based studies showed that PRMT6 depletion inhibits the proliferative capacity of CRC cells (data not shown), indicating other mechanisms potentially involved. Consistent with an impaired MMR capacity, PRMT6 loss exhibited a signature of active antitumor immune response, in which CD8⁺ and NK cells were increased, while PMN-MDSCs and/or M2 macrophages were reduced in colon tumors or xenografts. This observation supports a role of PRMT6 in antitumor immune response. To link the observed active immune response of PRMT6-depleted tumors to MMR defects, we have shown that PRMT6 loss induced cytosolic DNA accumulation and activation of the cGAS-STING pathway, which is consistent with what has been previously reported: that DNA sensing and activation of the cGAS-STING pathway in MHL1-deficient tumors is essential for antitumor immunity. Intriguingly, PRMT6-deleted cells showed a robust upregulation of IRF7 and ISG15, two important genes in response to MMR deficiency. It should be noted that MSH2 knockout did not completely reverse the increased expression of IRF7 and ISG15, and cGAS-STING activation caused by PRMT6 loss, indicating other mechanisms potentially involved. Previously, studies have showed that PRMT6 inhibits IRF3 binding to TBK1 to suppress antiviral innate immunity and type-I interferon production in bone marrow-derived macrophages. Although cell-specific functions and mechanisms frequently occur, PRMT6 might also function via IRF3-TBK1 to stimulate the cGAS-STING pathway and antitumor immunity in CRC, which remains an interesting topic for further investigation. Nevertheless, we have uncovered an alternative approach of PRMT6 to induce cGAS-STING activation via MMR defects and cytosolic DNA accumulation, at least partially.

We further showed that pharmacological inhibition of PRMT6 perturbed MutS α or MutS β complex assembly and suppressed MMR capacity in MSS CRC cells. Moreover, MSS CRC cells with a prolonged exposure to PRMT6Ti inhibitor maintained an MSI-like phenotype with impaired MMR activity. It is worth noting that MSH3 was also downregulated in MSS CRC cells in response to long-term treatment of PRMT6Ti inhibitor, an event that was seen in additional CRC cells with MSI, although of distinct MMR genes in different cells. These data suggested that PRMT6 regulates MMR transcriptionally. Previously, PRMT6 was reported to induce global DNA hypomethylation in cancer via preventing chromatin association with UHRF1, an accessory factor of DNA methyltransferases

DNMT1.⁴² It is possible that PRMT6 loss caused DNA hypermethylation that inactivates MMR gene expression, which remains to be determined in the future. Given the broad roles in cellular functions, including DNA repair, alternative splicing, DNA and histone methylation, long-term inhibition of PRMT6 might disrupt these processes in addition to MMR and lead to genomic instability and accumulation of DNA mutations within the cells, causing potential unintended effects, which may further increase the risk of secondary mutations or tumor evolution. This risk is particularly relevant for cancers with MSS, where the induction of an MSI-like phenotype might compromise genomic integrity over time. In the context of clinical translation, these findings highlight a dual-edged nature of PRMT6 inhibition and emphasize the importance of a balanced approach in translating PRMT6 inhibition into clinical practice.

As encouraged by an MSI-like phenotype caused by PRMT6 inhibitor, we next sought to determine whether PRMT6-mediated MSI-like phenotype has translational potential that would be sensitive to ICB therapy. Indeed, PRMT6 inhibition in MSS CT26 cells potentiates anti-PD1 efficacy, an effect that was not observed in MC38 cells, a MSI CRC cell line, indicating that PRMT6 inhibition facilitates ICB therapy by inducing an MSS-to-MSI conversion. The notion is further supported by the observations in AOM/DSS-induced colon tumors with MSS.

In conclusion, we have demonstrated that targeting PRMT6 using its inhibitor EPZ020411 in MMR-proficient CRC cells induces an MSI-like phenotype that shows sensitivity to immunotherapy. Therefore, our study provides a preclinical proof of concept to overcome resistance to immunotherapy by targeting PRMT6 in MSS CRC.

Author affiliations

¹Department of General Surgery, First Affiliated Hospital of Soochow University, Suzhou, Jiangsu, China

²Department of Pathology, Tongren Hospital Shanghai Jiaotong University School of Medicine, Shanghai, China

³Department of Biliary-Pancreatic Surgery, Shanghai Jiao Tong University, Shanghai, China

⁴Department of Clinical Laboratory, Shanghai Sixth People's Hospital, Shanghai, China

⁵Department of Clinical Laboratory, Shanghai 6th Peoples Hospital Affiliated to Shanghai Jiao Tong University, Shanghai, China

⁶Laboratory of Targeted Therapy and Precision Medicine, Department of Clinical Laboratory, Shanghai 6th Peoples Hospital Affiliated to Shanghai Jiao Tong University, Shanghai, China

⁷Department of General Surgery, Shanghai 6th Peoples Hospital Affiliated to Shanghai Jiao Tong University, Shanghai, China

Acknowledgments We greatly appreciate Professor Li Guo-Min at the University of Texas Southwestern Medical Center for providing the plasmid of GST-MSH2 as a gift.

Contributors YoZ, LG and YS conceived the ideas, designed the experiments, analyzed data, and wrote the manuscript. JD, YuZ and YS performed experiments and analyzed data. TC and QL performed sample collection and the clinical data analyses. JX and TL contributed to biochemical assays and animal experiments. TC and QL contributed to histological analysis and interpretation. YoZ contributed to graphical abstract preparation. All authors read and approved the final manuscript. YuZ, LG, and YS are responsible for the overall content as the guarantors.

Funding This work was supported by the Natural Science Foundation of Shanghai (23ZR1448600) and National Natural Science Foundation of China (82073258, 82472802).

Competing interests None declared.

Patient consent for publication Consent obtained from parent(s)/guardian(s).

Ethics approval Colorectal cancer (CRC) tissues were collected from Renji Hospital, School of Medicine, Shanghai Jiao Tong University. All experiments and analyses were conducted with the understanding and written consent of each participant. All manipulations were performed under the approval of the Research Ethics Committee of Renji Hospital, School of Medicine, Shanghai Jiao Tong University (RA-2024-343). For animal study, all procedures were performed with the approval of the Research Ethics Committee of the Shanghai Jiao Tong University Affiliated Sixth People's Hospital (22-0716).

Provenance and peer review Not commissioned; externally peer reviewed.

Data availability statement Data are available on reasonable request. The datasets used and analyzed during the current study are available from the corresponding author on reasonable request. The data of RNA-seq generated in this study can be viewed in NODE (<https://www.biosino.org/node>) by pasting the accession (OEZ00017581) into the search box.

Supplemental material This content has been supplied by the author(s). It has not been vetted by BMJ Publishing Group Limited (BMJ) and may not have been peer-reviewed. Any opinions or recommendations discussed are solely those of the author(s) and are not endorsed by BMJ. BMJ disclaims all liability and responsibility arising from any reliance placed on the content. Where the content includes any translated material, BMJ does not warrant the accuracy and reliability of the translations (including but not limited to local regulations, clinical guidelines, terminology, drug names and drug dosages), and is not responsible for any error and/or omissions arising from translation and adaptation or otherwise.

Open access This is an open access article distributed in accordance with the Creative Commons Attribution Non Commercial (CC BY-NC 4.0) license, which permits others to distribute, remix, adapt, build upon this work non-commercially, and license their derivative works on different terms, provided the original work is properly cited, appropriate credit is given, any changes made indicated, and the use is non-commercial. See <http://creativecommons.org/licenses/by-nc/4.0/>.

ORCID iD

Yonglong Zhang <http://orcid.org/0000-0001-6429-6304>

REFERENCES

- Morgan E, Arnold M, Gini A, *et al.* Global burden of colorectal cancer in 2020 and 2040: incidence and mortality estimates from GLOBOCAN. *Gut* 2023;72:338–44.
- Xie YH, Chen YX, Fang JY. Comprehensive review of targeted therapy for colorectal cancer. *Signal Transduct Target Ther* 2020;5:22.
- Oliveira G, Wu CJ. Dynamics and specificities of T cells in cancer immunotherapy. *Nat Rev Cancer* 2023;23:295–316.
- Sanmamed MF, Chen LP. A Paradigm Shift in Cancer Immunotherapy: From Enhancement to Normalization. *Cell* 2018;175:313–26.
- Nishino M, Ramaiya NH, Hatabu H, *et al.* Monitoring immune-checkpoint blockade: response evaluation and biomarker development. *Nat Rev Clin Oncol* 2017;14:655–68.
- André T, Shiu K-K, Kim TW, *et al.* Pembrolizumab in Microsatellite-Instability–High Advanced Colorectal Cancer. *N Engl J Med* 2020;383:2207–18.
- Overman MJ, McDermott R, Leach JL, *et al.* Nivolumab in patients with metastatic DNA mismatch repair-deficient or microsatellite instability-high colorectal cancer (CheckMate 142): an open-label, multicentre, phase 2 study. *Lancet Oncol* 2017;18:1182–91.
- Le DT, Kim TW, Van Cutsem E, *et al.* Phase II Open-Label Study of Pembrolizumab in Treatment-Refractory, Microsatellite Instability-High/Mismatch Repair-Deficient Metastatic Colorectal Cancer: KEYNOTE-164. *J Clin Oncol* 2020;38:11–9.
- Wensink GE, Elferink MAG, May AM, *et al.* Survival of patients with deficient mismatch repair metastatic colorectal cancer in the pre-immunotherapy era. *Br J Cancer* 2021;124:399–406.
- Bando H, Ohtsu A, Yoshino T. Therapeutic landscape and future direction of metastatic colorectal cancer. *Nat Rev Gastroenterol Hepatol* 2023;20:306–22.
- Westcott PMK, Sacks NJ, Schenkel JM, *et al.* Low neoantigen expression and poor T-cell priming underlie early immune escape in colorectal cancer. *Nat Cancer* 2021;2:1071–85.
- Ratovomanana T, Cohen R, Svrcek M, *et al.* Performance of Next-Generation Sequencing for the Detection of Microsatellite Instability in Colorectal Cancer With Deficient DNA Mismatch Repair. *Gastroenterology* 2021;161:814–26.
- Muzny DM, Bainbridge MN, Chang K. Comprehensive molecular characterization of human colon and rectal cancer. *Nature New Biol* 2012;487:330–7.
- André T, Tougeron D, Piessen G, *et al.* Neoadjuvant Nivolumab Plus Ipilimumab and Adjuvant Nivolumab in Localized Deficient Mismatch Repair/Microsatellite Instability-High Gastric or Esophagogastric Junction Adenocarcinoma: The GERCOR NEONIPIGA Phase II Study. *J Clin Oncol* 2023;41:255–65.
- Hu H, Kang L, Zhang J, *et al.* Neoadjuvant PD-1 blockade with toripalimab, with or without celecoxib, in mismatch repair-deficient or microsatellite instability-high, locally advanced, colorectal cancer (PICC): a single-centre, parallel-group, non-comparative, randomised, phase 2 trial. *Lancet Gastroenterol Hepatol* 2022;7:38–48.
- Li GM. Mechanisms and functions of DNA mismatch repair. *Cell Res* 2008;18:85–98.
- Ortega J, Lee GS, Gu LY, *et al.* Mismatch-bound human MutS–MutL complex triggers DNA incisions and activates mismatch repair. *Cell Res* 2021;31:542–53.
- Gupta S, Gellert M, Yang W. Mechanism of mismatch recognition revealed by human MutSβ bound to unpaired DNA loops. *Nat Struct Mol Biol* 2012;19:72–8.
- Bradford KC, Wilkins H, Hao PY, *et al.* Dynamic human MutSα–MutLα complexes compact mismatched DNA. *Proc Natl Acad Sci USA* 2020;117:16302–12.
- Vidula N, Lipman A, Kato S, *et al.* Detection of microsatellite instability high (MSI-H) status by targeted plasma-based genotyping in metastatic breast cancer. *NPJ Breast Cancer* 2022;8:117.
- Conibear AC. Deciphering protein post-translational modifications using chemical biology tools. *Nat Rev Chem* 2020;4:674–95.
- Li W, Li F, Zhang X, *et al.* Insights into the post-translational modification and its emerging role in shaping the tumor microenvironment. *Signal Transduct Target Ther* 2021;6:422.
- Christmann M, Tomicic MT, Kaina B. Phosphorylation of mismatch repair proteins MSH2 and MSH6 affecting MutSα mismatch-binding activity. *Nucleic Acids Res* 2002;30:1959–66.
- Bone KM, Wang P, Wu F, *et al.* NPM-ALK mediates phosphorylation of MSH2 at tyrosine 238, creating a functional deficiency in MSH2 and the loss of mismatch repair. *Blood Cancer J* 2015;5:e311.
- Zhang M, Xiang S, Joo H-Y, *et al.* HDAC6 deacetylates and ubiquitinates MSH2 to maintain proper levels of MutSα. *Mol Cell* 2014;55:31–46.
- Radhakrishnan R, Li YX, Xiang SY, *et al.* Histone deacetylase 10 regulates DNA mismatch repair and may involve the deacetylation of MutS homolog 2. *J Biol Chem* 2015;290:22795–804.
- Zhang M, Hu C, Tong D, *et al.* Ubiquitin-specific Peptidase 10 (USP10) Deubiquitinates and Stabilizes MutS Homolog 2 (MSH2) to Regulate Cellular Sensitivity to DNA Damage. *J Biol Chem* 2016;291:10783–91.
- Chan LH, Zhou L, Ng KY, *et al.* Abstract 4479: Protein arginine methyltransferase PRMT6 regulates cancer stemness through CRAF methylation in hepatocellular carcinoma. *Cancer Res* 2018;78:4479.
- Feng JW, Dang YP, Zhang WQ, *et al.* PTEN arginine methylation by PRMT6 suppresses PI3K–AKT signaling and modulates pre-mRNA splicing. *Proc Natl Acad Sci USA* 2019;116:6868–77.
- Huang T, Yang Y, Song X, *et al.* PRMT6 methylation of RCC1 regulates mitosis, tumorigenicity, and radiation response of glioblastoma stem cells. *Mol Cell* 2021;81:1276–91.
- Schneider L, Herkt S, Wang L, *et al.* PRMT6 activates cyclin D1 expression in conjunction with the transcription factor LEF1. *Oncogenesis* 2021;10:42.
- Wong TL, Ng KY, Tan KV, *et al.* CRAF Methylation by PRMT6 Regulates Aerobic Glycolysis-Driven Hepatocarcinogenesis via ERK-Dependent PKM2 Nuclear Relocalization and Activation. *Hepatology* 2020;71:1279–96.
- Zhang Y, Wang H, Chen T, *et al.* C24–Ceramide Drives Gallbladder Cancer Progression Through Directly Targeting Phosphatidylinositol 5-Phosphate 4-Kinase Type-2 Gamma to Facilitate Mammalian Target of Rapamycin Signaling Activation. *Hepatology* 2021;73:692–712.
- Chen T, Yuan ZQ, Lei Z, *et al.* Hippocalcin-Like 1 blunts liver lipid metabolism to suppress tumorigenesis via directly targeting RUVBL1–mTOR signaling. *Theranostics* 2022;12:7450–64.

- 35 Chen T, Jinlin D, Wang F, *et al.* GSTM3 deficiency impedes DNA mismatch repair to promote gastric tumorigenesis via CAND1/NRF2-KEAP1 signaling. *Cancer Lett* 2022;538:215692.
- 36 Shen JF, Ju ZL, Zhao W, *et al.* ARID1A deficiency promotes mutability and potentiates therapeutic antitumor immunity unleashed by immune checkpoint blockade. *Nat Med* 2018;24:556–62.
- 37 Nicolaides NC, Littman SJ, Modrich P, *et al.* A naturally occurring hPMS2 mutation can confer a dominant negative mutator phenotype. *Mol Cell Biol* 1998;18:1635–41.
- 38 Guan J, Lu C, Jin Q, *et al.* MLH1 Deficiency-Triggered DNA Hyperexcision by Exonuclease 1 Activates the cGAS-STING Pathway. *Cancer Cell* 2021;39:109–21.
- 39 Lu C, Guan J, Lu S, *et al.* DNA Sensing in Mismatch Repair-Deficient Tumor Cells Is Essential for Anti-tumor Immunity. *Cancer Cell* 2021;39:96–108.
- 40 Le DT, Durham JN, Smith KN, *et al.* Mismatch repair deficiency predicts response of solid tumors to PD-1 blockade. *Science* 2017;357:409–13.
- 41 Pan Q, Lou X, Zhang J, *et al.* Erratum: Genomic variants in mouse model induced by azoxymethane and dextran sodium sulfate improperly mimic human colorectal cancer. *Sci Rep* 2017;7:2784.
- 42 Veland N, Hardikar S, Zhong Y, *et al.* The Arginine Methyltransferase PRMT6 Regulates DNA Methylation and Contributes to Global DNA Hypomethylation in Cancer. *Cell Rep* 2017;21:3390–7.